Progress Report for SCEC award 19096
Interpreting crustal and lithospheric structure in the Eastern California Shear Zone underneath the Mojave Broadband Array

April 30, 2020

Investigators:
Thorsten Becker, UT Austin
Vera Schulte-Pelkum, CU Boulder

Collaborators:
Robert Porritt (UT Austin)
Wanying Wang (UT Austin)
Whitney Behr (ETH Zurich)

1. Project Overview

The project supported analysis of data from a high resolution, passive seismic array in the Mojave region. In May 2018, we deployed 19 broadband seismometers from the UT Austin UTIG quick deploy pool. The seismometers were deployed in a dense line, with interstation spacing of 2-4 km over the ~40 km line. The experiment is aimed at addressing two main questions: 1) What is the distribution of Eastern California Shear Zone strain below the seismogenic layer in the Mojave lithosphere, and how does this structure compare to more mature faults? And 2) How was the Mojave lithosphere modified in response to Laramide flat-slab subduction?

Stations were serviced and data retrieved in October 2019. We conducted teleseismic shear wave splitting and receiver function analysis, and initial results were presented at the 2019 September annual SCEC meeting. The results of this project will be used to evaluate fault loading beneath the Eastern California Shear Zone, and to help populate and test models of lithospheric structure and anisotropy for use in the SCEC Community Rheology, Velocity, and Stress Models.

SCEC Annual Science Highlights Exemplary Figure

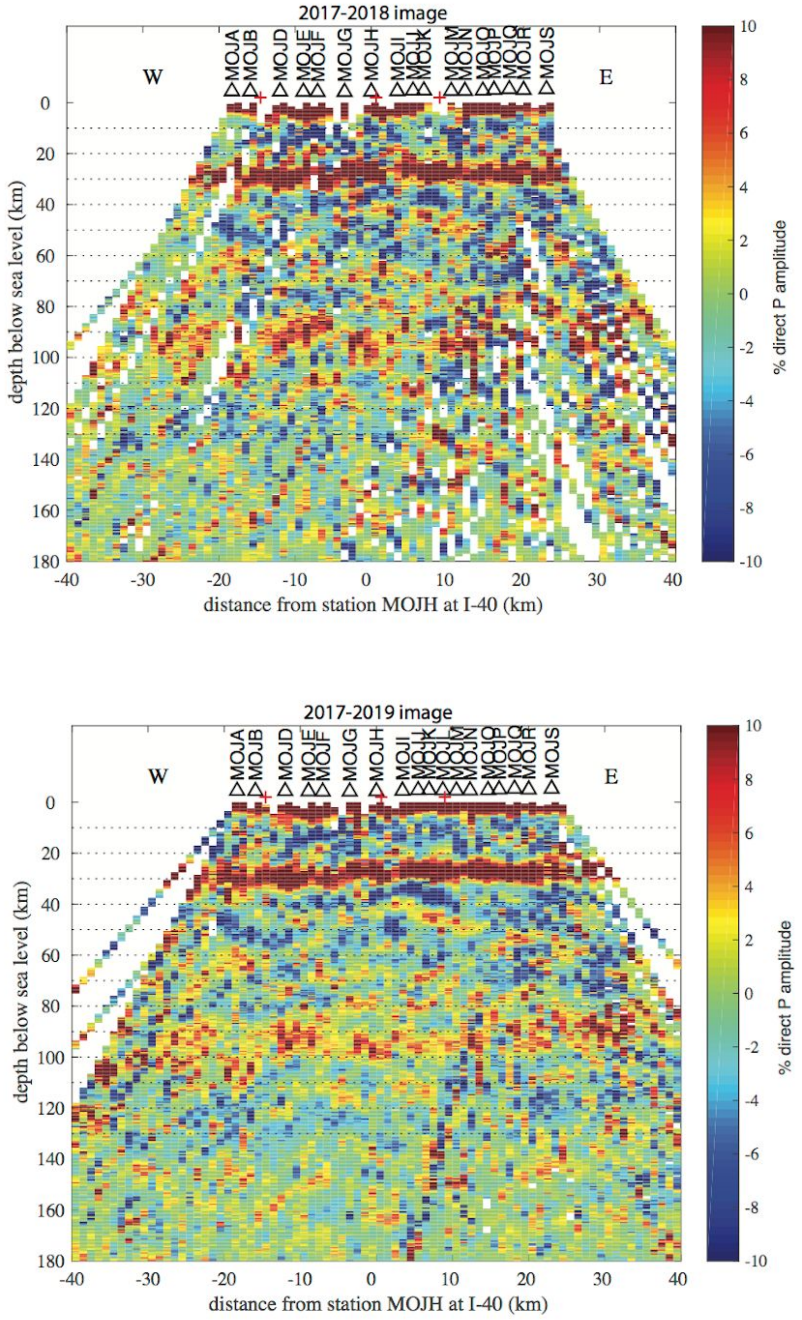

Figure 1: Common Conversion Point stacks of radial receiver functions using UT Austin's Mojave Broadband Array data from first (top) and second (bottom) service run. No smoothing is applied. Red crosses at the surface mark fault surface traces. The additional year of data filled in gaps seen in the early plot.

SCEC Science Priorities

3.b, 3.a, 1.b

Intellectual Merit

The Intellectual Merit associated with this project includes:

1. Better imaging of the deep fault structure and distribution of strain (localized vs. distributed) beneath the Eastern California Shear Zone, with implications for basal loading of upper crustal faults, postseismic relaxation, and earthquake cycle as well as fault evolution models.
2. Improved understanding of the Laramide lithospheric modification in the Mojave mantle lithosphere, including determining the composition of the lower crust (schist or no schist), the role of duplexing in the mantle lithosphere, and the hydration state of the lower crust and upper mantle, with implications (as above) for fault loading, postseismic relaxation, and earthquake cycle models.

Broader Impacts

Broader impacts include the following:

1. The high resolution seismic line focused on the Mojave region is complementary to efforts associated with developing the SCEC Community Rheology Model, particularly since the CRM community has identified the Mojave region as the ideal locality for implementing an initial version of the CRM.
2. The project leverages several additional sources outside of SCEC, including NSF grants awarded to all three PIs and UTIG funding via Becker's startup for the seismometer pool.
3. The work being conducted is highly interdisciplinary and will facilitate broad synthesis of a range of observations.
4. The project has already involved three UT undergraduate and three graduate students who assisted with the deployment and gained first hand experience in observational seismology.

Project Publications

Initial results were presented at the 2019 SCEC annual meeting.

2. Technical Report

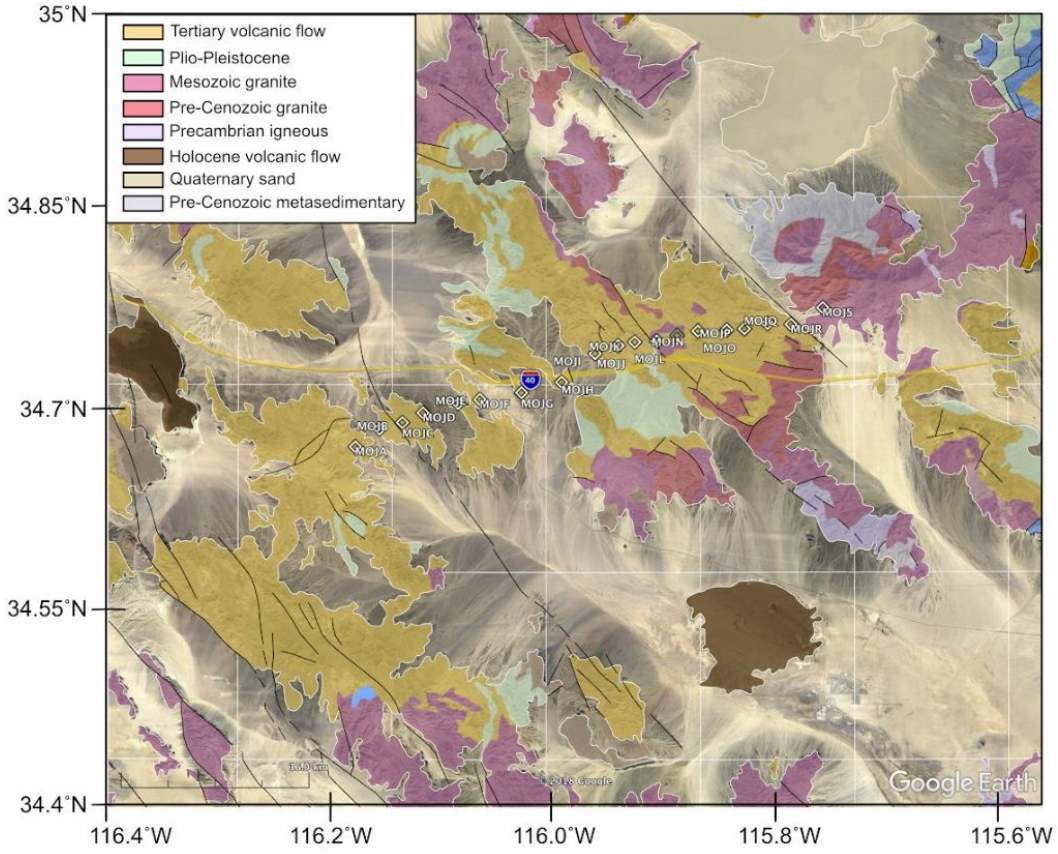

Figure 2: Geology of the study area, faults (black lines), and broadband stations (diamonds) deployed since May 2018.

Overview of General Project Goals

We seek to understand how plate-boundary deformation is accommodated in the lower crust and upper mantle in continental lithosphere which is fundamental to our understanding of fault systems. The partitioning of strain into specific rock constituents and the associated deformation mechanisms, for example, controls the relative contributions of different compositional layers to regional lithospheric strength, and the degree to which strain localizes at depth [e.g. Brace and

Kohlstedt, 1980; Kohlstedt et al., 1995]. It also determines under which conditions continental domains can be considered as relatively rigid blocks [e.g. McKenzie and Jackson, 1983; Avouac and Tapponnier, 1993; McCaffrey, 2005; Thatcher, 2009], partially decoupled crustal and mantle layers [e.g. McNutt et al., 1988; Burov and Diament, 1995], or a vertically uniform "thin viscous sheet" [e.g. England and McKenzie, 1982; Platt et al. 2008].

Observations of continental lithosphere deformation are typically indirect, sourced from a variety of techniques such as earthquake depth distributions [e.g. Molnar and Chen, 1982; Doser and Kanamori, 1986; Maggi et al., 2000; Sloan et al., 2011], potential field data [e.g. McGinnis et al., 1979; Tassara et al., 2007; Panet et al., 2010], observations of seismic velocities and anisotropy [e.g. Porter et al., 2011; Lin et al., 2010; Silver and Chan, 1991; Lev et al., 2006; Shapiro et al., 2004; Long and Becker, 2010], and viscoelastic models of displacements following large earthquakes and glacial or lake unloading [e.g. Thatcher, 1983; Bills et al., 1994; Burgmann and Dresen, 2008, Hearn & Thatcher, 2015]. Some actively deforming regions are, however, also host to young volcanoes that sample mantle and lower crustal material in the form of xenoliths; these can be used to place direct constraints on deep-seated deformation and to better constrain and complement larger-scale geophysical measurements [e.g. Titus et al., 2007; Behr and Hirth, 2014; Chatzaras et al., 2015; Behr and Smith, 2016].

The Mojave region in southeastern California is one such locality where a broad range of observations on lithospheric deformation has been collected, and where young volcanoes sample the lower crust and lithospheric mantle (Fig. 2). The region has experienced several Cordilleran tectonic events over the Cenozoic, including Laramide flat-slab subduction in the late Cretaceous [Barth and Schneiderman, 1996; Saleeby, 2003], followed by significant E-W-oriented lithospheric extension and associated volcanism from the early Miocene through the late Pleistocene [Glazner et al., 1989, 2002]. Currently, the Mojave region straddles the boundary between San Andreas transform-related deformation and Basin and Range extension and is host to a distributed network of NW-SE-striking strike-slip faults known as the Eastern California Shear Zone [ECSZ; e.g. Dokka and Travis, 1990]. The protracted Cenozoic history and modern-day tectonic activity in the area has likely produced complex deformation patterns, both old and new, in the deep crust and lithospheric mantle that both geophysical and xenolith studies can help to tease apart. It is a key region where slip is transferred along the plate boundary off the main fault [e.g. Savage et al., 2001; Meade and Hager, 2005; Becker et al., 2005; Platt and Becker, 2010; Chuang and Johnson 2011], but its role in the future evolution of the plate boundary is unclear [e.g. Herbert et al., 2016; Evans et al., 2016; Thatcher et al., 2016]. The relative richness of background datasets, including post-seismic studies [e.g. Freed and Burgmann, 2004; Pollitz et al., 2001], the relatively well constrained geologic history, and the relevance to California seismic hazard, make the Mojave an important place to study the progressive modification of the lithosphere in response to evolving plate motions. Permanent seismic stations

are scarce (Fig. 2), but new seismological observations pertaining to the downward continuation of faults in the ECSZ could be usefully compared to similar efforts of densely imaging other cross sections on the San Andreas fault.

Our goal in this project is to conduct initial analysis of data from the high resolution, passive seismic array in the Mojave region. The deployment is aimed at addressing two main questions that are fundamental to understanding the geologic framework and mechanical behavior of the Mojave lithosphere: 1) What is the distribution of ECSZ strain below the seismogenic layer in the Mojave lithosphere? 2) How was the Mojave lithosphere modified in response to Laramide flat-slab subduction?

Summary of Work Conducted During this Funding Cycle

Seismometers were serviced and data retrieved and processed in Fall 2019. The data were submitted to the IRIS DMC. In the following, we provide a brief outline of some of the preliminary results from the data analysis.

Receiver function analysis

Figure 1 shows Common Conversion Point stacks for data from the 2018 and 2019 service runs. The additional year of data fills in gaps in ray coverage. The Moho has a generally smooth appearance with apparent crustal thickness variations in the west, which may be real or due to lower crustal velocities in the west compared to the east (a 1-D model was used for depth migration). Slight topography may be present on the Moho; its appearance will be clearer when further data being collected this year are included. We also expect further improvement from stacking down artifacts, already visible in Fig. 1.

Figure 3 shows results from an initial analysis of plunging axis anisotropy and dip signals in receiver functions. The method [Schulte-Pelkum and Mahan, 2014a,b] maps the depth and strike of contrasts in plunging axis anisotropy (foliation strike) or of dipping boundaries between isotropic layers. We display the depth and strike of the largest amplitude arrival in Fig. 3. We observed a gradient from deeper arrivals in the west to shallower on average in the east. Strikes are close to surface fault strikes, but appear to vary especially in the eastern half of the array. There is a possible contrast between E-W strikes deeper and N-S strikes shallower in the eastern half of the line. We expect further stabilization of results as more events from this year are incorporated after the next service run.

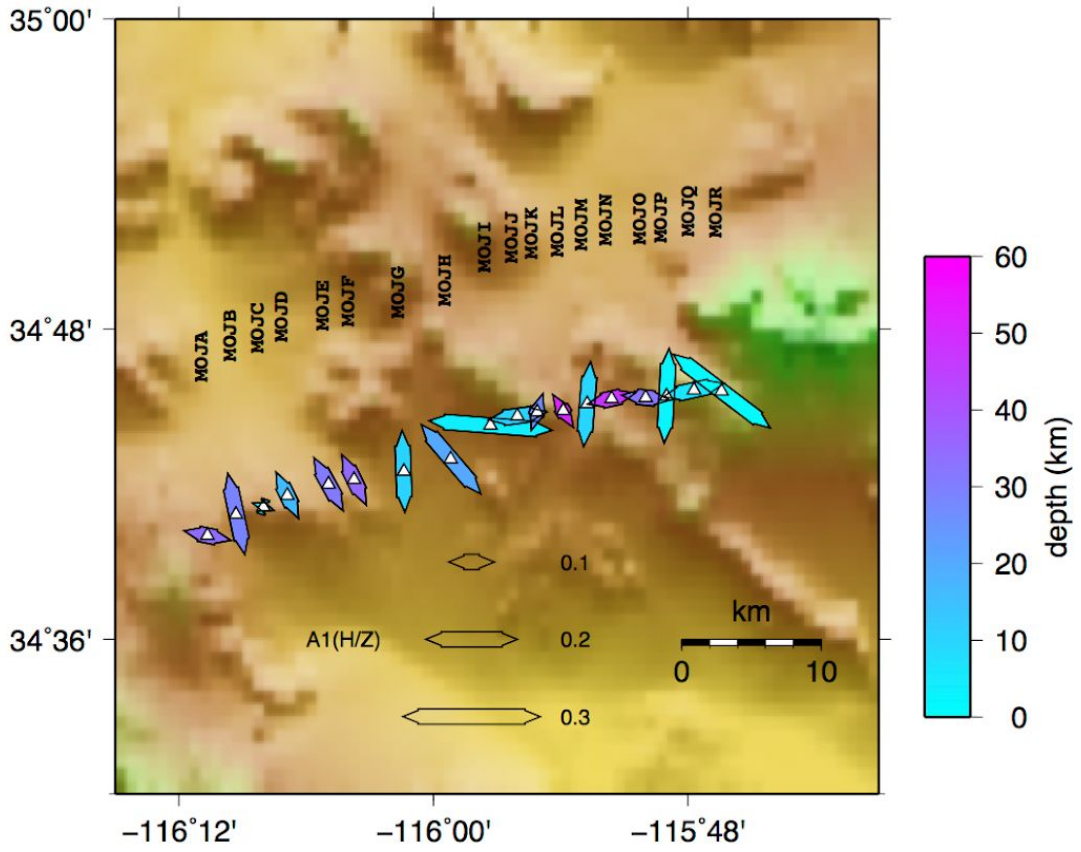

Figure 3: Maximum first azimuthal harmonic arrival (A1max) at each station. Fill color is depth of the converter, orientation of the arrow is strike of the converting contrast in dipping foliation or dipping contrast between isotropic layers, and arrow length is amplitude of the arrival, which scales with strength and dip of the contrast.

Teleseismic shear wave splitting analysis

Manual shear wave splitting measurements were made with *SplitLab* [*Wüstefeld et al.*, 2008]. We visually determined ~20-30 second time windows around *SKS* arrivals as predicted by the 1-D velocity model IASP91 [*Kennett,* 1991] and checked filter bands of 10 to 100 seconds and 5 to 50 seconds for splitting analysis. This analysis evaluates three different splitting algorithms (rotation correlation, transverse energy minimization, and eigenvalue method) and the user assigns a quality metric of good, fair, or poor based on similarity of results and other diagnostic plots. After these measurements are made, a station average is computed stacking the misfit spaces of delay time vs. fast azimuth and searching for the minimum misfit.

To further constrain the results, we also conduct shear wave splitting analysis using *SplitRacer* [*Reiss and Rümpker,* 2017], which provides consistency in measuring the entire dataset through a recently implemented automatic quality categorization approach [*Link and Rümpker,* 2019]. The splitting parameters are measured using the transverse energy minimization method. The measurements are then categorized as good, average, poor, and null based on the energy reduction on the transverse component, splitting intensity, and cross correlation analysis. All events are pre-processed with the same filter bandwidth and a fixed signal to noise ratio. Since the filter could affect the measurements, we test filter bands of 1 to 100 seconds, 2 to 50 seconds, 2 to 80 seconds and 4 to 50 seconds. Station averaged orientations and delay times are computed to compare to the *SplitLab* results.

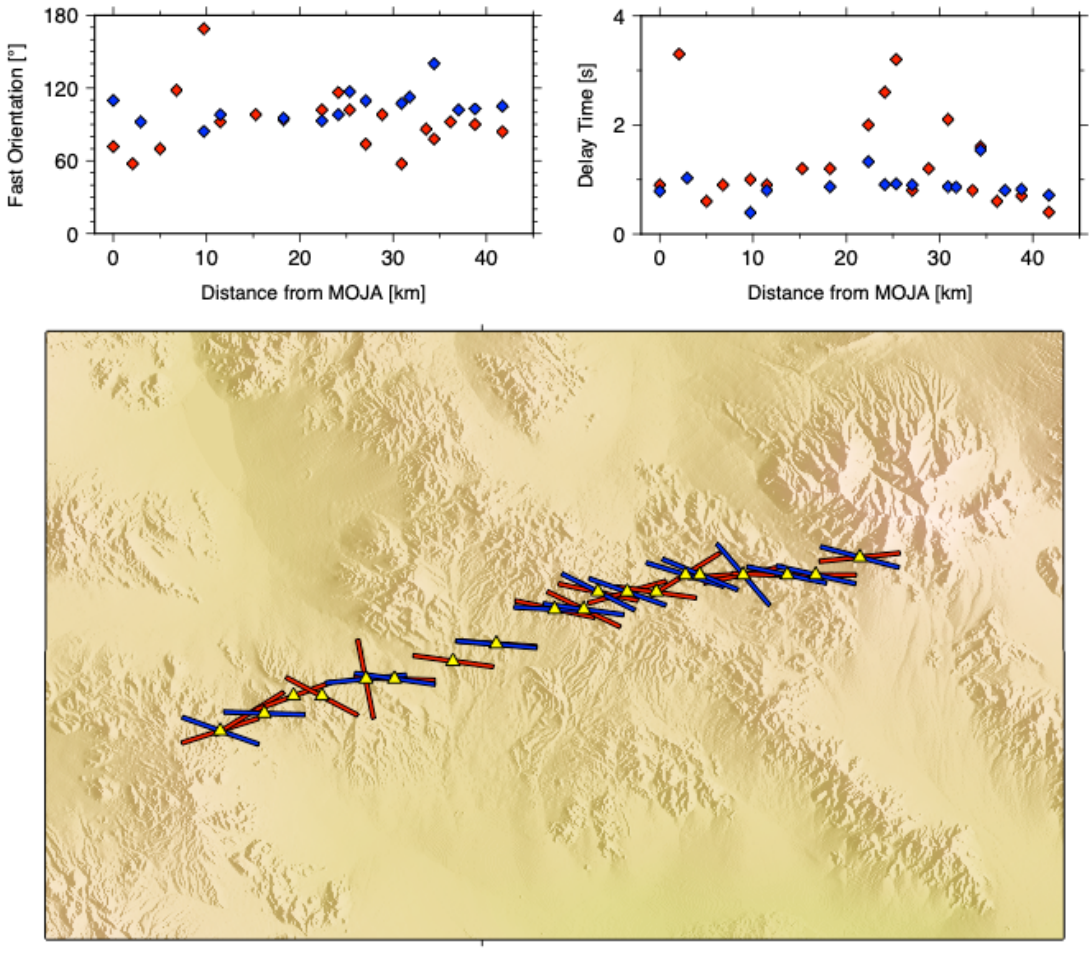

Figure 4: Station averaged splitting parameters from the transverse energy minimization method. *SplitRacer* (*SplitLab*) result is shown by blue (red) diamond/vector. (Top left) Values of fast orientation along strike. Distance on the horizontal axis is counted from an origin point at the

westernmost station, MOJA (cf. Fig. 2). (Top right) Values of delay time along strike. (Bottom) The comparison between *SplitRacer* and *SplitLab* results.

Planned Future Activities

PIs Becker and Schulte-Pelkum and UTIG grad student Wang and researcher Porritt will continue to conduct analysis of the profile data, perform receiver function analysis, put receiver function results in the regional deep deformation field context based on SCEDC permanent station data, including rock fabric and shear zone imaging at depth using the method developed by Schulte-Pelkum and Mahan [2014a,b], assess site data quality, and conduct *S* and *SKS* splitting measurements as well as anisotropic receiver function analysis.

References

Allam, A. A., Y. Ben-Zion I. Kurzon and F. L. Vernon, 2014. Seismic velocity structure in the Hot Springs and Trifurcation Seismicity Cluster Areas of the San Jacinto Fault Zone from double-difference tomography, Geophys. J. Int., 198, 978–999, doi: 10.1093/gji/ggu176.

Barak, S. and Klemperer, S.L., 2016. Rapid variation in upper-mantle rheology across the San Andreas fault system and Salton Trough, southernmost California, USA. Geology, 44(7), 575-578.

Chapman, A., 2017. The Pelona–Orocopia–Rand and related schists of southern California: a review of the best-known archive of shallow subduction on the planet, INTERNATIONAL GEOLOGY REVIEW, 59, 5–6, 664–701, http://dx.doi.org/10.1080/00206814.2016.1230836.

Dorsey, R. J., G. J. Axen, T. C. Peryam, and M. E. Kairouz, 2012. Initiation of the Southern Elsinore Fault at ~1.2 Ma: Evidence from the Fish Creek–Vallecito Basin, southern California, Tectonics, 31, TC2006, doi:10.1029/2011TC003009.

Dumond, G., K. H. Mahan, M. L. Williams, M. J. Jerkovic, 2013. Transpressive uplift and exhumation of continental lower crust revealed by synkinematic monazite reactions, Lithosphere 5, 507-512, doi: 10.1130/L292.1.

Freed, A.M. and Bürgmann, R., 2004. Evidence of power-law flow in the Mojave desert mantle. Nature, 430(6999), pp.548-551.

Hauksson, E., W. Yang, and P. M. Shearer, 2012. Waveform Relocated Earthquake Catalog for Southern California (1981 to June 2011), Bulletin of the Seismological Society of America, Vol. 102, No. 5, pp. 2239–2244, October 2012, doi: 10.1785/0120120010.

Inbal, A., Ampuero, J.P. and Clayton, R.W., 2016. Localized seismic deformation in the upper mantle revealed by dense seismic arrays. Science, 354(6308), 88-92.

Kennett B.L.N., 1991. IASPEI 1991 Seismological Tables, Research School of Earth Sciences, Australian National University.

Long, M. and T. Becker, 2010. Mantle dynamics and seismic anisotropy, EPSL 297, 341-354, doi:10.1016/j.epsl.2010.06.036.

Mason, C. C., Spotila, J. A., Axen, G., Dorsey, R. J., Luther, A., & Stockli, D. F., 2017. Two-phase exhumation of the Santa Rosa Mountains: Low- and high-angle normal faulting during initiation

and evolution of the southern San Andreas Fault system. Tectonics, 36, 2863–2881. https://doi.org/10.1002/2017TC004498.

Miller, M.S., Zhang, P. and Dolan, J.F., 2014. Moho structure across the San Jacinto fault zone: Insights into strain localization at depth. Lithosphere, 6(1), 43-47.

Ozakin, Y. and Y. Ben-Zion, 2015. Systematic receiver function analysis of the Moho geometry in the Southern California plate-boundary region, Pure Appl. Geophys., 172, 1167-1184, doi:10.1007/s00024-014-0924-6.

Pollitz, F.F., Wicks, C. and Thatcher, W., 2001. Mantle flow beneath a continental strike-slip fault: Postseismic deformation after the 1999 Hector Mine earthquake. Science, 293(5536), pp.1814-1818.

Porter, R., Zandt, G. and McQuarrie, N., 2011. Pervasive lower-crustal seismic anisotropy in Southern California: Evidence for underplated schists and active tectonics. Lithosphere, 3, 201-220.

Schulte-Pelkum, V. and Y. Ben-Zion, 2012. Apparent vertical Moho offsets under continental strike-slip faults from lithology contrasts in the seismogenic crust, Bull. Seis. Soc. Am., 102(6), 2757-2763, doi: 10.1785/0120120139.

Schulte-Pelkum, V. and K. Mahan, 2014a. Imaging faults and shear zones using receiver functions, Pure Appl. Geophys., 171 (2014), 2967–2991, doi: 10.1007/s00024-014-0853-4.

Schulte-Pelkum, V., K. Mahan, 2014b. A method for mapping crustal deformation and anisotropy with receiver functions and first results from USArray, Earth Planet. Sci. Lett., 402, 221-233.

Sibson, R. H., 1983. Continental fault structure and the shallow earthquake source, J. geol. Soc. London, 140, 741-767.

Takeuchi, C. S, Y. Fialko, 2012. Dynamic models of interseismic deformation and stress transfer from plate motion to continental transform faults, JGR 117, B05403, doi:10.1029/2011JB009056.

Tatham, D. J., Lloyd, G. E., Butler, R. W. H., Casey, M., 2008. Amphibole and lower crustal seismic properties., Earth and Planetary Science Letters 267, 118-1.

Ward, D., K. Mahan, V. Schulte-Pelkum, 2012. Roles of quartz and mica in seismic anisotropy of mylonites, Geophys. J. Int., 190(2), 1123-1134, doi:10.1111/j.1365-246X.2012.05528.x.

Wüstefeld, A., G. Bokelmann, C. Zaroli, and G. Barruol (2008), SplitLab: A shear-wave splitting environment in Matlab. *Computers & Geosciences*, 34 (5), p. 515-528. doi:10.1016/j.cageo.2007.08.002.

Zhu, L., 2000. Crustal structure across the San Andreas Fault, southern California from teleseismic converted waves, EPSL 179, 183-190.